Departamento de Física .UBAexactas

ATTOSECOND PHYSICS

UNIT XI ATTOSECOND STREAKING

Diego Arbó
diego.arbo@uba.ar

1st Semester 2024, Buenos Aires, Argentina

Departamento de Física .UBAexactas

THE STREAKING PRINCIPLE

STREAK CAMERA

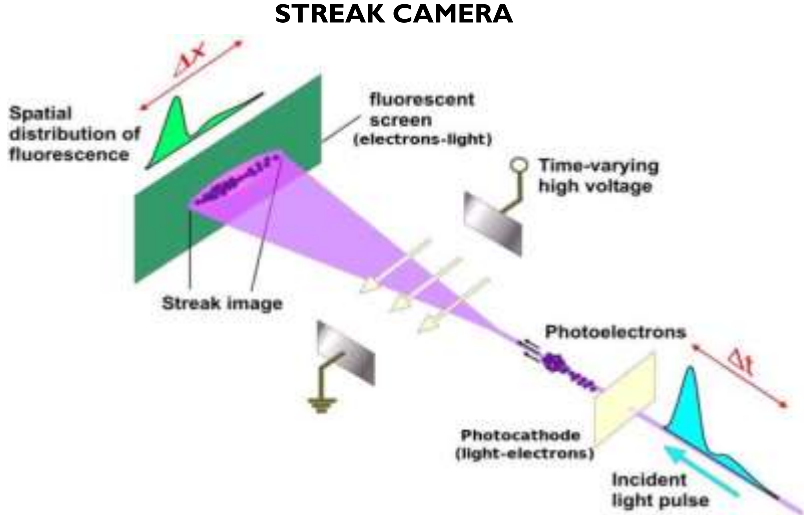

Conventional optoelectronic streak camera where the photoelectrons are deflected by a linearly ramped on electric field and thus time is mapped to spatial displacement on the screen. Maximal resolution ~ picoseconds.

THE STREAKING PRINCIPLE

ATTOSECOND STREAKING IN STRONG-FIELD APPROXIMATION

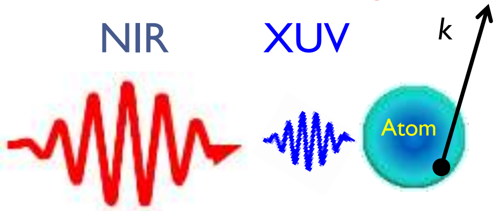

Linearly polarized
in the same direction

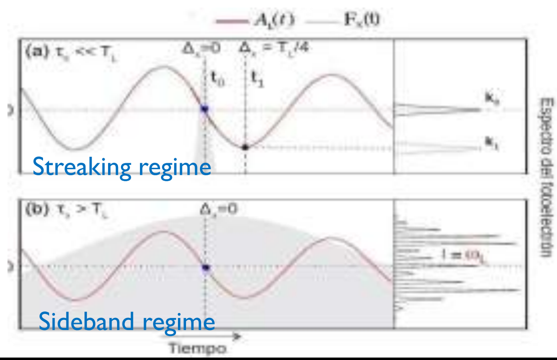

THE STREAKING PRINCIPLE

$$\mathbf{F}(t) = \mathbf{F}_X(t) + \mathbf{F}_L(t)$$

The XUV pulse is responsible for the single-photon ionization

$$p_0 = \sqrt{2(\hbar\omega_{\text{XUV}} - I_p)}$$

The IR laser deflects the photoelectron.
It works as the DC field in streak camera.

$$\frac{d\vec{p}}{dt} = -F_L(t)$$

$$\vec{k} = \vec{p}(t=\infty) = \vec{p}_0 - \int_{t_i}^{\infty} \vec{F}_L(t)dt = \vec{p}_0 - \left[-\vec{A}_L(\infty) + \vec{A}_L(t_i)\right]$$

$$\mathbf{A}(t) = -\int_0^t dt' [\mathbf{F}_X(t') + \mathbf{F}_L(t')] = \mathbf{A}_L(t) + \underbrace{\mathbf{A}_X(t)}_{\ll 1} \simeq \mathbf{A}_L(t)$$

THE STREAKING PRINCIPLE

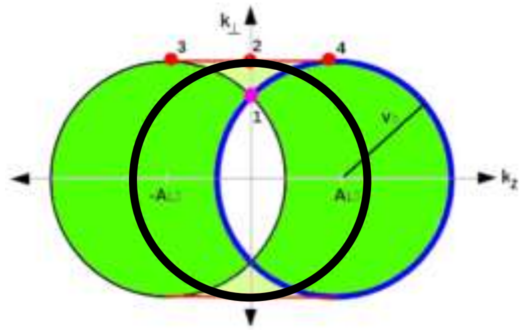

$$\vec{k} = \vec{p}_0 - \vec{A}_L(t_i)$$

Fundamental equation of streaking

Recording a set of spectra for different delay times between the XUV and IR field yields a streaking spectrogram which is a direct representation of the vector potential of the IR field.

CHARACTERIZATION OF ULTRASHORT LIGHT PULSES

In 2004 the oscillation of visible light could be directly measured for the first time by attosecond streaking.

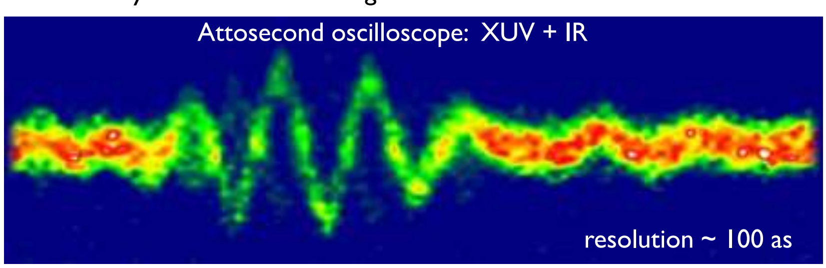

E. Goulielmakis *et al*, Science **305**, 1267 (2004)

Typical streaking laser fields. IR laser field with λ = 800nm, a sine-squared envelope and total duration of 6 fs and an intensity of $I_{IR} = 4 \cdot 10^{11}$W/cm^2. The XUV pulse has a Gaussian envelope and a FWHM duration of 200 as and an intensity $I_{XUV} = 10^{13}$W/cm^2.

Attosecond streaking has become a basic tool for the characterization of ultrashort light pulses as well as of the duration and chirp of attosecond pulses.

Departamento de Física .UBAexactas

STREAKING TIME

Beyond the SFA: Streaking spectrogram for ionization of helium with and without excitation of the second electron (lower and upper structure). For reference the vector potential $A(\tau\,)$ is shown in red. Comparison of the shift of the spectrogram yields the streaking time shifts (see inset).

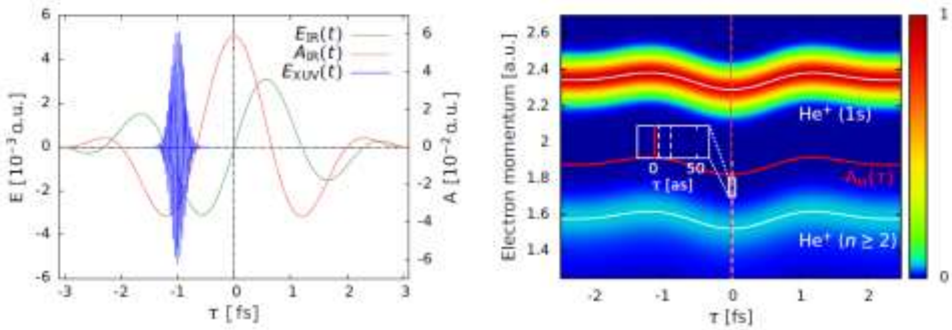

If the electron is emitted delayed by t_S it will feel a slightly different vector potential and the streaking spectrogram will be phase shifted with respect to the vector potential.
Thus, we can extract the absolute time shifts by a nonlinear least-squares fit of the modified final momentum k to the vector potential A(t).

Departamento de Física .UBAexactas

STREAKING TIME

Attosecond streaking works as a classical clock

$$\vec{k} = \vec{p}_0 - \alpha \vec{A}_L(t - t_S)$$

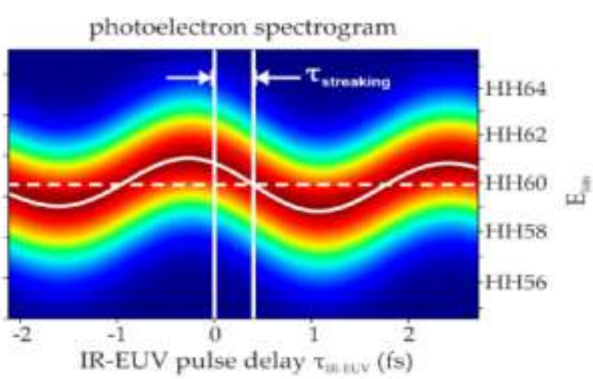

Exercise 18: Calculate the correction factor and the streaking time $\mathbf{t_S}$ for the amplitude of the momentum shift induced by the streaking field using a Taylor expansion up to first order of the preceding equation.

Departamento de Física
.UBAexactas

IAFE CONICET UBA

EFFECT OF THE DURATION OF THE XUV PULSE

Streaking spectrograms for ionization from the hydrogen ground state for different XUV pulse durations τ_X, ω = 80 eV and I_X = 10^{13}W/cm^2. The IR field had a total duration of 6 fs with a sine-squared envelope, λ = 800nm and I_L = 10^{12}W/cm^2. The duration of one optical cycle is 2668 as. The spectra are taken in forward direction with an opening angle of 10°.

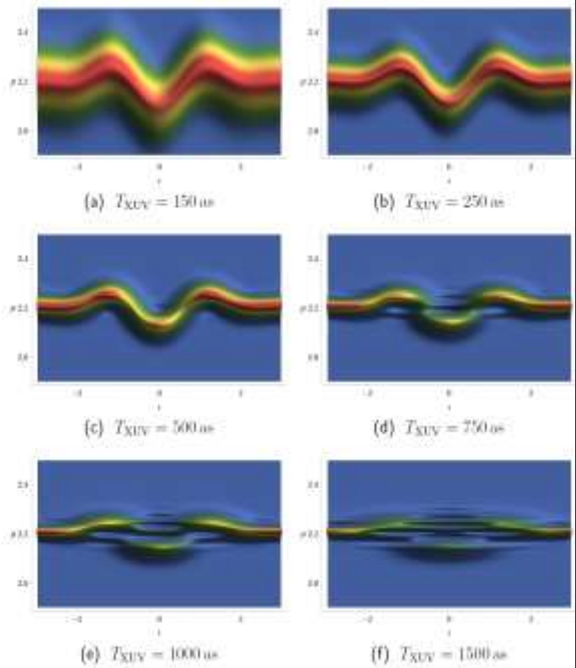

Departamento de Física
.UBAexactas

IAFE CONICET UBA

LASER ASSISTED XUV IONIZATION

The sampled vector potential is averaged over the temporal width of the XUV pulse, i.e., the relative momentum shift is to first order given by a convolution of the vector potential and the ionization probability

$$\Delta \mathbf{p}_f(\tau) \approx \frac{1}{I_{\text{tot}}} \int_{-\infty}^{\infty} |E_{\text{XUV}}(t-\tau)|^2 \, \mathbf{A}_{\text{IR}}(t) \mathrm{d}t$$

$$I_{\text{tot}} = \int_{-\infty}^{\infty} |E_{\text{XUV}}(t-\tau)|^2 \, \mathrm{d}t$$

The extracted energy-dependent time delays $t_S(E)$ are averaged over the spectral width of the XUV pulse

$$t_S(E) \approx \frac{1}{I_{\text{tot}}} \int_{-\infty}^{\infty} \left| \tilde{E}_{\text{XUV}}(\omega - I_p - E) \right|^2 t_S(\omega - I_p) \mathrm{d}\omega$$

Departamento de Física .UBA exactas

IAFE CONICET UBA

LASER ASSISTED XUV IONIZATION

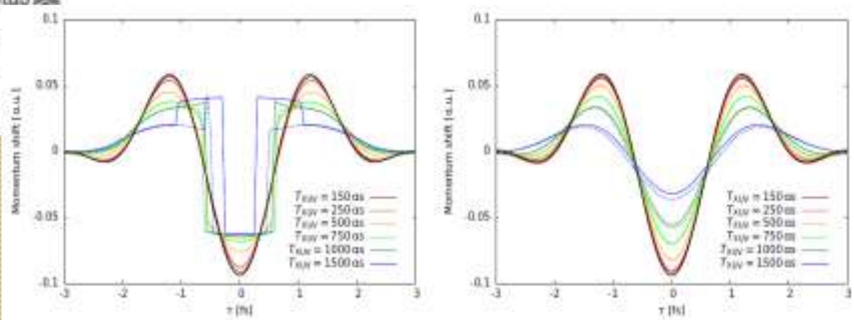

(a) Peak position (b) First moment

Momentum shift in forward (solid lines) and in backward (dotted lines) direction along the laser polarization axis extracted by either the maximum (a) or the first moment (b) of the streaked spectra. For pulse durations longer than a quarter IR period (667 as) the peak analysis gets discontinuous, the first moment, however, follows the vector potential with a reduced amplitude until an XUV pulse duration of 1500 as.

Departamento de Física .UBA exactas

IAFE CONICET UBA

LASER ASSISTED XUV IONIZATION

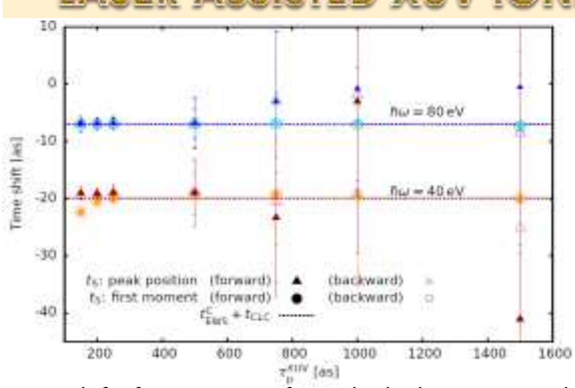

Extracted streaking time shifts for ionization from the hydrogen ground state for two different XUV energies ($\hbar\omega$ = *80* eV, red/orange points and $\hbar\omega$ = *40* eV, blue points) as a function of the XUV pulse duration. We compare time shifts extracted by the peak maximum (filled and open triangles, forward and backward direction analysis, respectively) and by the first moment (filled and open circles) with a theoretical prediction based on Coulomb EWS time delay and a contribution due to the long-ranged character of the Coulomb field. Although the errors from the fit get larger, the first moment analysis is remarkably stable until 1500 as.
The peak analysis already breaks down for 750 as

Departamento de Física .UBAexactas

CONICET

SHORT-RANGE POTENTIALS

We compare the following three time delays:

(i) The wavepacket delay $t_{WP} = t - \langle r(t) \rangle / k$ (extracted from the extrapolation of the wavepacket trajectory to a linear slope that starts at t_{WP} from the origin) as a function of propagation time,

(ii) The EWS delay averaged over the spectral width of the wavepacket $\langle t_{EWS} \rangle$ and

(i) The streaking delays that we extract by a nonlinear least-squares fit of the first moment of the streaking spectrogram to the vector potential of the IR field.

Departamento de Física .UBAexactas

CONICET

SHORT-RANGE POTENTIALS

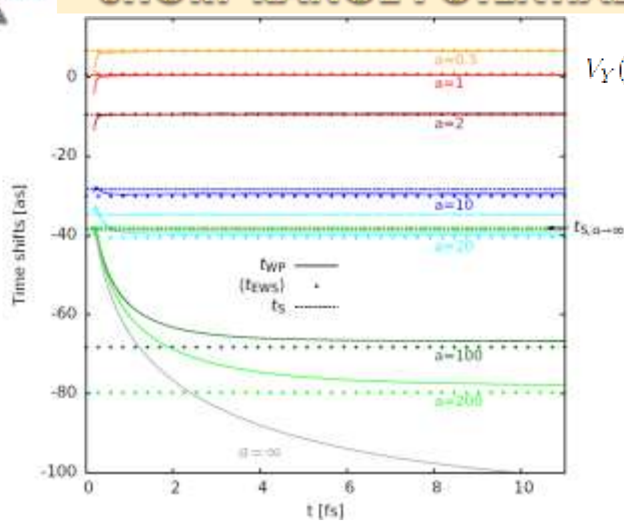

$$V_Y(r) = -\frac{Z}{r} e^{-r/a}$$

For Yukawa potentials with screening lengths $a \lesssim 10$ a.u. we find that the extracted streaking time shifts t_S for the given laser parameters indeed agree exactly with the intrinsic atomic time shifts $\langle t_{EWS} \rangle$. The wavepacket delay t_{WP} also converges to $\langle t_{EWS} \rangle$ shortly after the ionizing XUV field is over.

Departamento de Física
UBA exactas
IAFE CONICET UBA

SHORT-RANGE POTENTIALS

For sufficiently short-ranged potentials (a few a.u.) the electrons emission time (arrival in the continuum) is delayed by the EWS time, i.e., the ponderomotive momentum *A(t)* to be shifted by t_{EWS}, $A(t + t_{EWS})$.

$$t_S = t_{WP} = \langle t_{EWS} \rangle \approx t_{EWS}$$

$$\vec{k} = \vec{p}_0 - \vec{A}_L(t - t_S) = \vec{p}_0 - \vec{A}_L(t - t_{EWS})$$

For Yukawa potentials with larger screening lengths ($a \gtrsim 10$ a.u.) the streaking time shifts t_S no longer agree with t_{EWS} and t_{WP} .

The extracted streaking time shifts are always less negative than t_{EWS}, and, moreover, they converge to the streaking time shift for a pure Coulomb potential, $t_{S,\, a\to\infty}$, for screening lengths $a \gtrsim 100$ a.u.

Conclusion:

Streaking is only able to extract intrinsic atomic time shifts that are built-up within a distance of a few atomic units and that for potentials with longer range, in particular for Coulomb potentials some modifications are necessary.

Departamento de Física
UBA exactas
IAFE CONICET UBA

SHORT-RANGE POTENTIALS

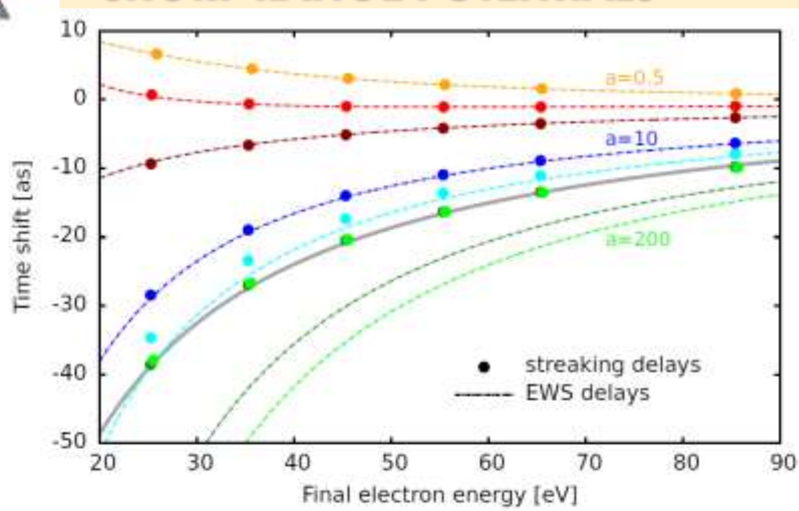

Streaking and EWS time shifts for the Yukawa potentials (a = *0.5, 1, 2, 10, 20, 100, 200* a.u.) as a function of the electron energy E. t_S agrees with t_{EWS} for small a and converges for large a to t_S of a Coulomb potential with Z = 2 (grey solid line).

Departamento de Física
.UBAexactas

COULOMB-LASER COUPLING

Since for easily resolvable energy shifts IR fields with intensities of the order $I_L \sim 10^{11}–10^{12}$ W/cm^2 are needed, distortion effects generally cannot be neglected.

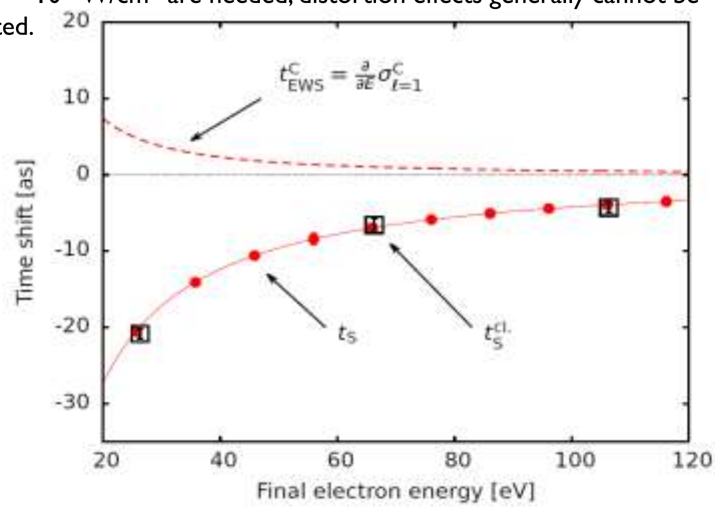

t_S (red dots) agrees well with the classical streaking time shift $t^{cl}{}_S$ (black boxes) calculated with the CTMC method.

Departamento de Física
.UBAexactas

COULOMB-LASER COUPLING

Since for easily resolvable energy shifts IR fields with intensities of the order $I_L \sim 10^{11}–10^{12}$ W/cm^2 are needed, distortion effects generally cannot be neglected.

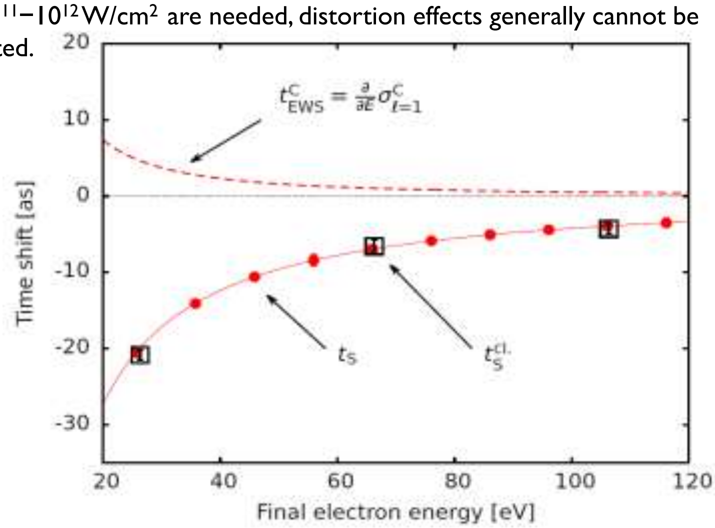

t_S (red dots) agrees well with the classical streaking time shift $t^{cl}{}_S$ (black boxes) calculated with the CTMC method.

COULOMB-LASER COUPLING

We consider a typical trajectory of outgoing electrons. Since the Coulomb force depends on the trajectory *r(t)*, for an exact treatment we need to solve the differential equation for a trajectory taking off at $r(t_i) \approx 0$ near the ionic core in the combined Coulomb and laser fields,

$$\ddot{\vec{r}}(t) = a_{C+IR}\left[r(t)\right]$$

$$\dot{\vec{r}}(t) = \dot{\vec{r}}(t_0) + \int_{t_0}^{t} a_{C+IR}\left[r(t')\right]dt'$$

$$\vec{k} = \dot{\vec{r}}(\infty) = \dot{\vec{r}}(t_0) + \int_{t_0}^{\infty} a_{C+IR}\left[r(t')\right]dt'$$

In the SFA: $\vec{k} = \dot{\vec{r}}(t_0) + \int_{t_i}^{\infty} a_{IR}(t)dt = \vec{p}_0(t_0) - \vec{A}_L(t_0)$

In absence of the IR laser: $\vec{p}_0 = \dot{\vec{r}}(\infty) = \dot{\vec{r}}(t_0) + \int_{t_0}^{\infty} dt a_C(r(t)) = \sqrt{2\left(\omega_X - I_p\right)}$

COULOMB-LASER COUPLING

$$\vec{k} = \dot{\vec{r}}(t_0) + \int_{t_0}^{\infty} a_{C+IR}\left[\vec{r}(t)\right]dt$$

$$\vec{k} = \vec{p}_0 + \int_{t_0}^{\infty} \left\{a_{C+IR}\left[\vec{r}(t)\right] - a_C\left[\vec{r}(t)\right]\right\}dt$$

$$\vec{k} = \vec{p}_0 - \vec{A}(t_0) + \int_{t_0}^{\infty} \left\{a_{C+IR}\left[\vec{r}(t)\right] - a_C\left[\vec{r}(t)\right] - a_{IR}\left[\vec{r}(t)\right]\right\}dt$$

$$\int_{\tau}^{t(R_{\text{cut}})} \left(a_{C+\text{IR}}\left[\vec{r}(t)\right] - a_C\left[\vec{r}(t)\right] - a_{\text{IR}}\left[\vec{r}(t)\right]\right)dt = c_{\text{short}}(\epsilon, Z, L)F_{\text{IR}}(\tau)\,.$$

$$\int_{t(R_{\text{cut}})}^{\infty} \left(a_{C+\text{IR}}\left[\vec{r}(t)\right] - a_C\left[\vec{r}(t)\right] - a_{\text{IR}}\left[\vec{r}(t)\right]\right)dt = c_{\text{asym}}(\epsilon, Z, \omega_{\text{IR}})F_{\text{IR}}(\tau)\,.$$

Departamento de Física
UBA exactas
IAFE CONICET UBA

COULOMB-LASER COUPLING

$$\vec{p}_f(\tau) = \vec{p}_0 - \vec{A}_{IR}(\tau + t^{C,\,cl.}_{EWS} + t_{CLC})$$

$$t^{C,\,cl.}_{EWS} = \frac{1}{\omega_{IR}} \tan^{-1}\left[\omega_{IR} c_{short}(\epsilon, Z, L)\right]$$

$$t_{CLC} = \frac{1}{\omega_{IR}} \tan^{-1}\left[\omega_{IR} c_{asym}(\epsilon, Z, \omega_{IR})\right]$$

$$c_{short}(\epsilon, Z, L) = \frac{1}{\omega_{IR}} \tan\left(\frac{\omega_{IR} Z}{(2\epsilon)^{3/2}} \ln\left(\sqrt{\eta^2 + L^2}\right)\right)$$

$$c_{asym}(\epsilon, Z, \omega_{IR}) = \frac{1}{\omega_{IR}} \tan\left(\frac{\omega_{IR} Z}{(2\epsilon)^{3/2}} \ln\left(\epsilon T_{IR}\right)\right)$$

$$t_S = t^{C}_{EWS}(\epsilon, \ell, Z) + t_{CLC}(\epsilon, Z, \omega_{IR})$$

t_{CLC} is universal for Coulomb exit channel interactions, i.e., is independent of the atomic species and initial state.

Departamento de Física
UBA exactas
IAFE CONICET UBA

COULOMB-LASER COUPLING

Since the Coulomb-laser coupling is of classical origin, we can determine t_{CLC} classically by subtracting the classical limit of the EWS time delay from the classical streaking time determined by the CTMC,

$$t_{CLC}(E) = t^{cl.}_{S}(E, L) - t^{C,\,cl.}_{EWS}(E, L)$$

$$t^{C,\,cl.}_{EWS}(E, L) = \frac{Z}{k^3} \ln\left(\sqrt{\eta^2 + L^2}\right)$$

$$\begin{aligned} t_{Coul}(E, \ell, r) &= \frac{\partial}{\partial E}\left(\frac{Z}{k}\ln(2kr) + \sigma_\ell(E)\right) \\ &= \Delta t_{Coul}(E, r) + t^{C}_{EWS}(E, \ell) \end{aligned}$$

➔ $\Delta t_{Coul} = t_{CLC}$

Departamento de Física
.UBAexactas

COULOMB-LASER COUPLING

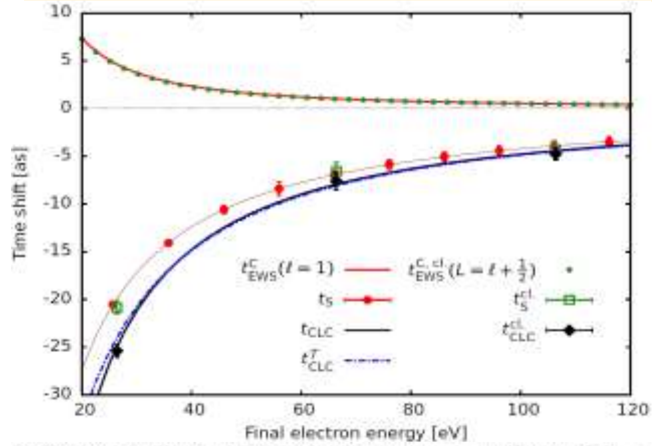

Photoionization of H(1s) by an XUV pulse ($I_{XUV} = 10^{13}\,\mathrm{W/cm^2}$, $\tau_p = 200\,\mathrm{as}$) as a function of E ($E = \omega_{XUV} + \varepsilon_{1s}$) streaked by an IR field with $I_{IR} = 10^{12}\,\mathrm{W/cm^2}$, $\omega_{IR} = 0.057$ a.u. (800 nm). Shown are both the quantum and classical EWS delay time and the streaking time t_S. Classical and quantum t_{CLC} determined by subtraction (Eq. 4.24) agree with each other to within the graphical resolution when taking into account that the classical angular momentum corresponding to a quantum wave with well defined ℓ is $L = \ell + \frac{1}{2}$. The analytic estimate t^{T}_{CLC}, Eq. 4.30, coincides as well.

Departamento de Física
.UBAexactas

EXPERIMENTS

NATURE | VOL 419 | 24 OCTOBER 2002 | www.nature.com/nature

Time-resolved atomic inner-shell spectroscopy

M. Drescher*†, M. Hentschel*, R. Kienberger*, M. Uiberacker*, V. Yakovlev*, A. Scrinzi*, Th. Westerwalbesloh†, U. Kleineberg†, U. Heinzmann† & F. Krausz*

* Institut für Photonik, Technische Universität Wien, Gusshausstrasse 27, A-1040 Wien, Austria
† Fakultät für Physik, Universität Bielefeld, Universitätsstrasse 25, D-33615 Bielefeld, Germany

The characteristic time constants of the relaxation dynamics of core-excited atoms have hitherto been inferred from the linewidths of electronic transitions measured by continuous-wave extreme ultraviolet or X-ray spectroscopy. Here we demonstrate that a laser-based sampling system, consisting of a few-femtosecond visible light pulse and a synchronized sub-femtosecond soft X-ray pulse, allows us to trace these dynamics directly in the time domain with attosecond resolution. We have measured a lifetime of $7.9^{+1.0}_{-0.9}$ fs of M-shell vacancies of krypton in such a pump–probe experiment.

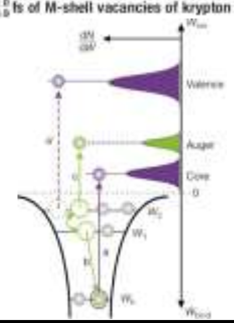

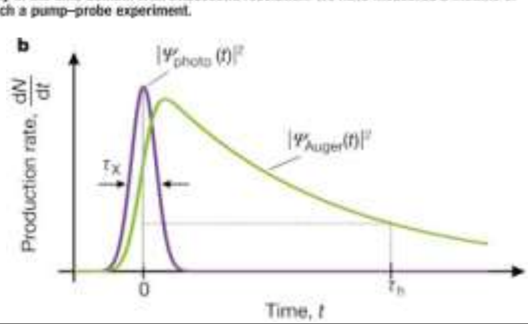

Departamento de Física
.UBAexactas

EXPERIMENTS

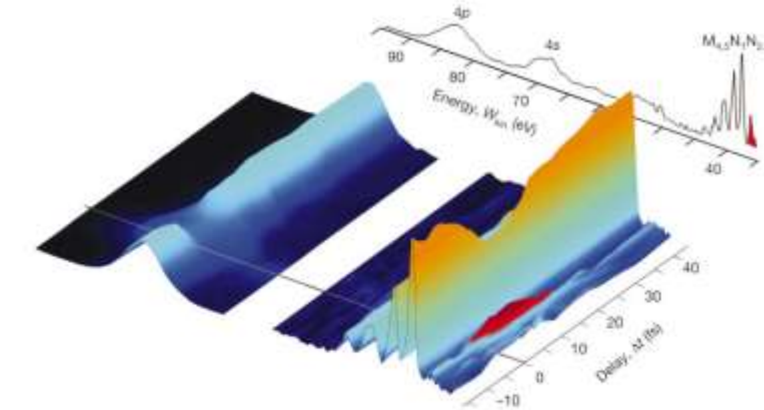

Figure 4 Evolution of electron spectra following core excitation. The spectra were recorded after the exposure of krypton atoms to a 97-eV sub-femtosecond X-ray pulse and a sub-7-fs, 750-nm laser pulse at different delays between the pulses. The surface plot shows the evolution of the 4*p* photo line and the $M_{4,5}N_1N_{2,3}$ Auger lines with Δt. The spectrum highlighted in the background was recorded at $\Delta t = 5$ fs. According to equation (1) the kinetic energy spectrum of the sub-laser-cycle-duration photo electrons (4*s* and 4*p* lines) should be periodically shifted versus Δt. However, for τ_x comparable to $T_0/2$ this periodic shift merges to a continuous broadening (probing the laser amplitude envelope $E_a(t)$) owing to the absence of stabilization of the absolute phase φ in our laser pulses, because light pulses with $\varphi \approx 0$ and $\varphi \approx \pi$ induce shifts of opposite sign and turn asymmetric shifts into symmetric broadening. The laser peak intensity was evaluated from the broadening of photo lines as $I_0 \approx 5\times10^{11}$ W cm^{-2}. The evolution of the first-order sideband (highlighted in red) of the lowest-energy member of the $M_{4,5}N_1N_{2,3}$ Auger group reflects the delayed decay dynamics of the krypton 3*d* core hole. A pronounced positive temporal shift of the side-band maximum with respect to the photo-line minimum is clearly discernible (see also Fig. 5).

Departamento de Física
.UBAexactas

EXPERIMENTS

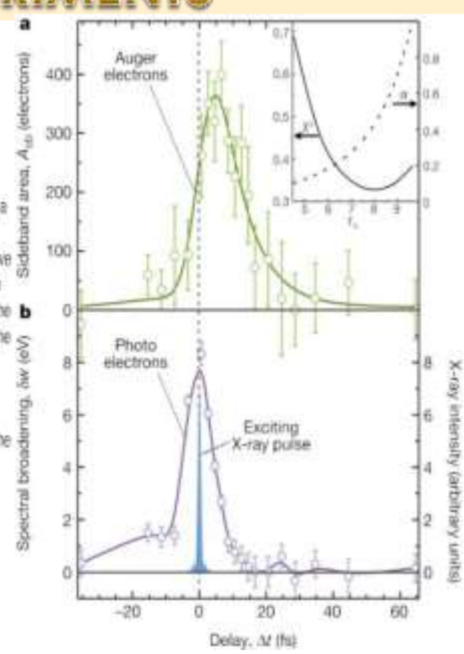

Figure 5 Probing the temporal evolution of Auger electron emission. **a**, Sideband area (circles) of the first-order sideband of the lowest-energy Kr $M_{4,5}N_1N_{2,3}$ Auger line extracted from the spectra of Fig. 4 and a fitted convolution of the exponential decay curve $R_0\int \exp[-(t-t')/\tau_h]|E_a^2(t')|dt'$ with a power 2α of the amplitude envelope of the laser field. Because $\tau_X \ll \tau_L$, the latter is proportional to the spectral broadening of the 4*p* photoline from the same electron spectrum, presented in **b**. Panel **b** also displays the temporal intensity profile of the X-ray pulse computed from its measured energy distribution (FWHM ≈ 3 eV) assuming the absence of chirp, which applies to cut-off harmonic radiation under our experimental conditions as was verified in a recent experiment[6]. Inset, the confidence band for τ_h is confined by the merit function χ^2 and the valid range of α to $\tau_h = 7.9^{+1.0}_{-0.9}$ fs.

Departamento de Fisica
.UBAexactas

EXPERIMENTS

25 JUNE 2010 VOL 328 SCIENCE www.sciencemag.org

Delay in Photoemission

M. Schultze,[1,2]* M. Fieß,[2] N. Karpowicz,[2] J. Gagnon,[1,2] M. Korbman,[2] M. Hofstetter,[1] S. Neppl,[3] A. L. Cavalieri,[2] Y. Komninos,[4] Th. Mercouris,[4] C. A. Nicolaides,[4] R. Pazourek,[5] S. Nagele,[5] J. Feist,[5,6] J. Burgdörfer,[5] A. M. Azzeer,[7] R. Ernstorfer,[3] R. Kienberger,[2,3] U. Kleineberg,[2] E. Goulielmakis,[2] F. Krausz,[1,2] V. S. Yakovlev[1,2]*

Photoemission from atoms is assumed to occur instantly in response to incident radiation and provides the basis for setting the zero of time in clocking atomic-scale electron motion. We used attosecond metrology to reveal a delay of 21 ± 5 attoseconds in the emission of electrons liberated from the 2*p* orbitals of neon atoms with respect to those released from the 2*s* orbital by the same 100–electron volt light pulse. Small differences in the timing of photoemission from different quantum states provide a probe for modeling many-electron dynamics. Theoretical models refined with the help of attosecond timing metrology may provide insight into electron correlations and allow the setting of the zero of time in atomic-scale chronoscopy with a precision of a few attoseconds.

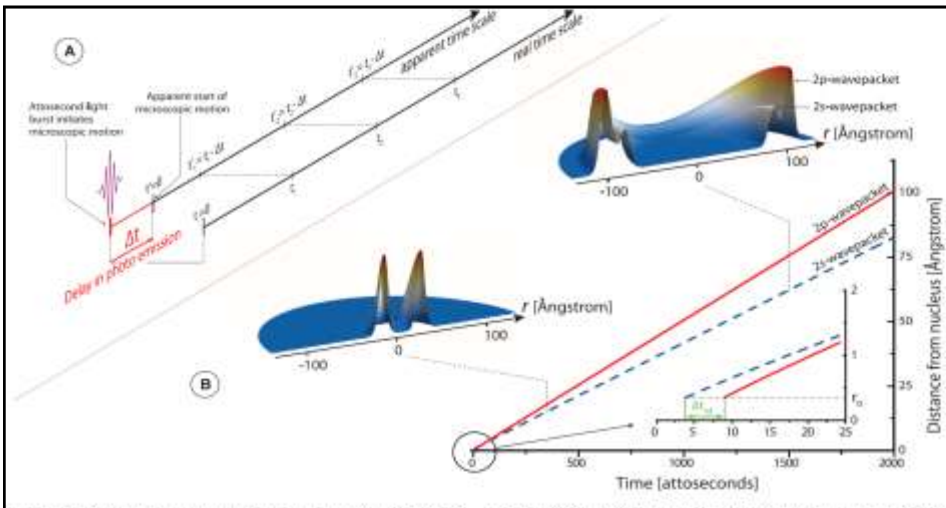

Fig. 1. Attosecond delay in photoemission and its consequences. (**A**) The "real" time scale begins at the maximum of the XUV pulse, whereas the "apparent" time scale in the measurement starts with the release of an electron wave packet and is temporally shifted by a possible delay Δt in photoemission. A delay between the arrival time of the attosecond XUV excitation pulse and the instant of emission would falsify the conclusions reached from measurements with an atomic chronoscope, which is triggered by the emission of an electron wave packet. A microscopic event that occurred at $t = t_{real}$ is indicated by this chronoscope to have apparently happened at $t' = t_{real} - \Delta t$, thereby tainting a comparison between theory and experiment with an unknown systematic error of Δt. (**B**) The surface plots show the spatial distribution of the photoelectron density around the atomic core at $t_1 = 300$ as and $t_2 = 1500$ as after the maximum of the XUV pulse, evaluated by solving the time-dependent Schrödinger equation with the aid of the state-specific expansion approach. As time progresses, the wave packets released from the 2*s* and 2*p* subshells become spatially separated because of their different velocities. Far from the nucleus, where the overlap with ionic orbitals is negligible, their motion can be described semi-classically. Therefore, knowing the average position and velocity of a wave packet that propagates toward the detector, we can illustrate a possible delay in its emission by tracing a classical electron trajectory back to the ion. The red solid and blue dashed lines show the classical trajectories of the 2*p* and 2*s* photoelectrons, respectively. The lines terminate at a distance $r_s = 0.3$ Å, which is equal to the radius of the valence shell. At this distance, the trajectories behave as if they started with a relative delay $\Delta t_{rel} = 5$ as, which is in reasonable agreement with the value obtained by a more rigorous theoretical analysis.

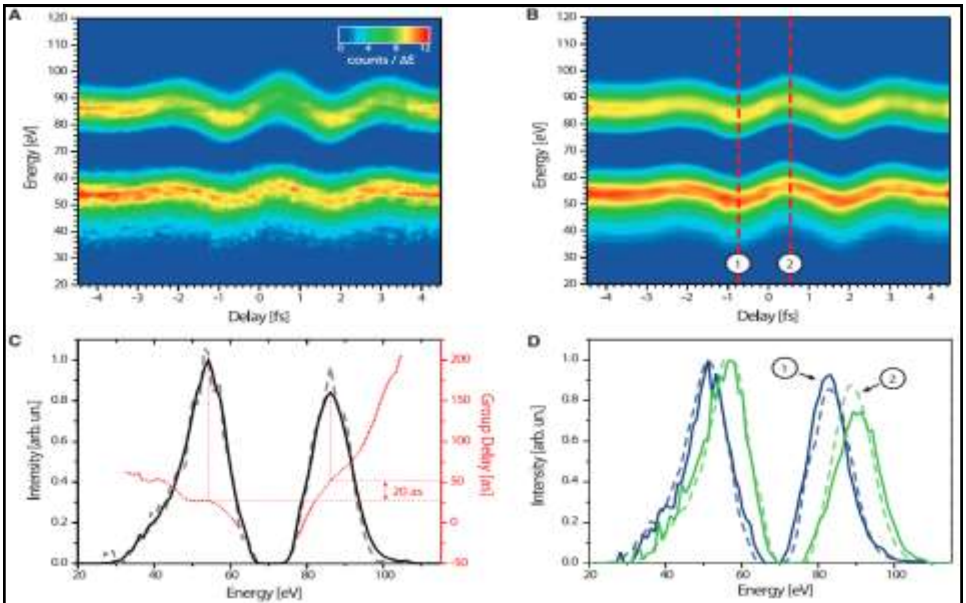

Fig. 2. Attosecond streaking spectrograms (**A** and **B**), evaluated photoelectron wave packets (**C**), and streaked spectra (**D**). The spectrograms in (A) are composed of a series of photoelectron energy spectra recorded by releasing 2*s* and 2*p* electrons from Ne with an attosecond XUV pulse in the presence of a strong NIR few-cycle laser field, as a function of the delay between the XUV and NIR fields. The spectrogram is processed with a FROG algorithm tailored for streaking measurements (*30*). (B) shows the spectrogram reconstructed by this algorithm. The retrieved 2*s* and 2*p* spectra, together with the respective group delays, are plotted in (C) (black solid line and red dotted line, respectively). The reconstructed energy spectra are in excellent agreement with the measured ones (gray dashed line). The average difference between the group delays corresponds to a 20-as retardation of the 2*p* emission with respect to the 2*s* emission. (D) compares reconstructed and measured streaked spectra at two delays, which exhibit the largest positive and negative shifts of the electron energy distribution.

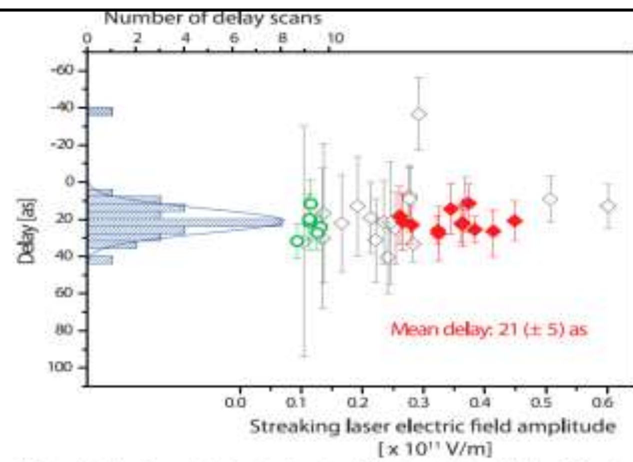

Fig. 3. The relative delay between photoemission from the 2*p* and 2*s* subshells of Ne atoms, induced by sub–200-as, near–100-eV XUV pulses. The depicted delays are extracted from measured attosecond streaking spectrograms by fitting a spectrogram, within the strong-field approximation, with parameterized NIR and XUV fields. Our optimization procedure matches the first derivatives along the time delay dimension of the measured and reconstructed spectrograms, thereby eliminating the influence of unstreaked background electrons [for details on the fitting algorithm, see (*29*)]. From the analysis of a set of spectrograms, the measured delays and associated retrieval uncertainties are plotted against the amplitude of the vector potential applied in the attosecond streak camera. Spectrograms measured in the presence of a satellite attosecond pulse were found to exhibit a less accurate retrieval of the delay value. When a subset of data (red diamonds) that represents scans with less than 3% satellite pulse content was evaluated, a mean delay value of 21 as with a standard deviation of ~5 as was found. The green circles represent the result of analyzing spectrograms recorded with an XUV pulse with narrower bandwidth in order to exclude the potential influence of shakeup states contributing to the electron kinetic energy spectrum.

Departamento de Física .UBAexactas

ATTOSECOND ANGULAR STREAKING

Attoclock

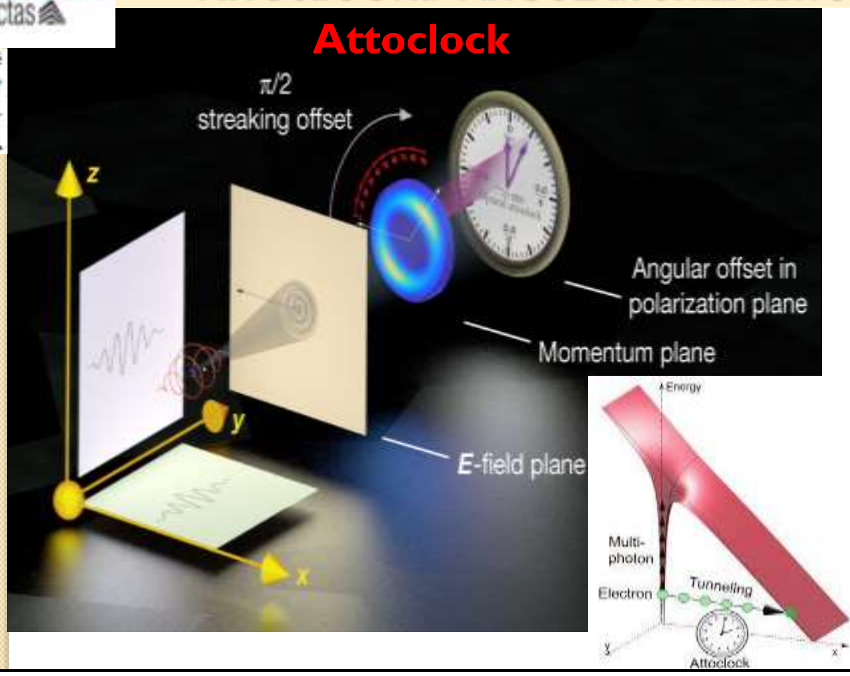

Departamento de Física .UBAexactas

ATTOSECOND ANGULAR STREAKING

Circularly polarized NIR laser

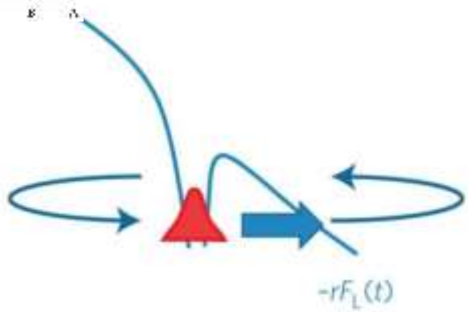

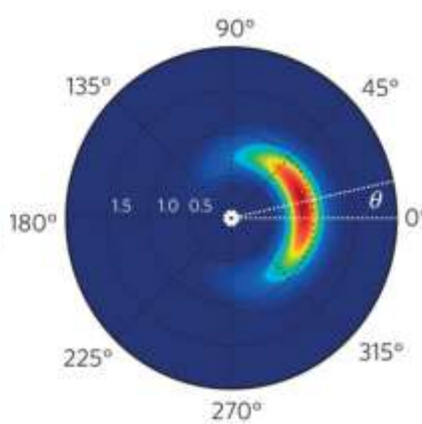

$$\tau = \theta / \omega$$

Departamento de Física
.UBAexactas

ATTOSECOND ANGULAR STREAKING

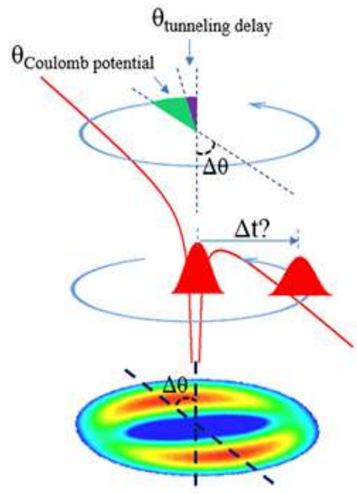

$\Delta\theta = \theta_{\text{Coulomb potential}} + \theta_{\text{tunneling delay}}$

- An offset angle $\Delta\theta$ of photoelectron momentum distribution can be measured experimentally.
- This offset angle comes from the tunneling delay ($\theta_{\text{tunneling delay}}$) and Coulomb potential effect （$\theta_{\text{Coulomb potential}}$）.
- The tunneling delay can be achieved only if $\theta_{\text{Coulomb potential}}$ have been determined.